Improved Limit on the Branching Ratio of $\mu \rightarrow e$ Conversion on Lead

W. Honecker, C. Dohmen, H. Haan, D. Junker, G. Otter, M. Starlinger, and P. Wintz*
III. Physikalisches Institut B der RWTH Aachen, D-52056 Aachen, Germany

J. Hofmann
Institut für Teilchenphysik der ETH Zürich, CH-5232 Villigen PSI, Switzerland

W. Bertl, J. Egger, and B. Krause†
Paul Scherrer Institut, CH-5232 Villigen PSI, Switzerland

S. Eggli, R. Engfer, Ch. Findeisen, E. A. Hermes, T. Kozlowski,‡ C. B. Niebuhr,§ H. S. Pruys, and A. van der Schaaf
Physik-Institut der Universität Zürich, CH-8057 Zürich, Switzerland

(SINDRUM II Collaboration)

(Received 13 July 1995)

The SINDRUM II spectrometer at Paul Scherrer Institute is used in a search for coherent $\mu \rightarrow e$ conversion in muonic atoms. We report on a measurement on lead, which resulted in $\Gamma(\mu^- \mathrm{Pb} \rightarrow e^- \mathrm{Pb}^{\mathrm{g.s.}})/\Gamma(\mu^- \mathrm{Pb\ capture}) < 4.6 \times 10^{-11}$ (90% C.L.). This upper limit improves on the previous value by an order of magnitude. Combined with the limit on titanium, it is interpreted in terms of phenomenological couplings between the lepton current and the isoscalar and isovector quark currents.

PACS numbers: 25.30.–c, 11.30.Fs, 24.80.+y, 36.10.Dr

Lepton flavor seems to be conserved in all particle interactions. Despite intensive efforts searches for processes like $\mu^+ \rightarrow e^+\gamma$, $K_L^0 \rightarrow \mu e$, or $Z^0 \rightarrow \mu\tau$ resulted in upper limits only. Lepton-flavor conservation (LFC) holds absolutely in the standard model as a consequence of vanishing neutrino masses. LFC, however, is not forced by a known gauge symmetry and in many generalizations of the standard model violations may be expected [1–3].

Neutrinoless $\mu \rightarrow e$ conversion, $\mu^-(A, Z) \rightarrow e^-(A, Z)$, in muonic atoms with mass number A and atomic number Z offers one of the most sensitive tests of LFC [4–8]. Muonic atoms decay by either muon decay in orbit or nuclear muon capture. The capture probability f_{capt} increases as Z does and reaches a value of 0.97 for lead, which corresponds to a lifetime of 75 ns [9]. It has been estimated [10] that $\mu \rightarrow e$ conversion would leave the nucleus in its ground state with a probability of more than 80%. Only this *coherent* fraction can be measured without background from bound muon decay.

Following Shanker [11] the branching ratio $B_{\mu e}(A, Z) \equiv \Gamma_{\mu e}(A, Z)/\Gamma_{\mathrm{capt}}(A, Z)$ for coherent $\mu \rightarrow e$ conversion is written as the sum of an isoscalar ($i = 0$) and an isovector ($i = 1$) contribution:

$$B_{\mu e}(A, Z) = \left(g_{V,S}^0 + g_{V,S}^1 \frac{Z - N}{3A}\right)^2 \frac{\Gamma_{V,S}(A, Z)}{\Gamma_{\mathrm{capt}}(A, Z)}, \quad (1)$$

where V and S denote vector and scalar interactions, respectively, and $N = A - Z$. The reduced widths $\Gamma_V(A, Z)$ and $\Gamma_S(A, Z)$ have been calculated from muon and electron wave functions and nucleon densities assuming G_F as a coupling constant and are tabulated in Ref. [11]. Recent calculations [10] predict a maximum for $B_{\mu e}$ in the region around lead, assuming vector interaction with typical, model-dependent values (5/6 or 3) for the ratio of the coupling constants g_V^1/g_V^0. Presently, the best constraints on g^0 and g^1 come from the limits (90% C.L.)

$$\begin{aligned} B_{\mu e}^{\mathrm{S}} &< 7 \times 10^{-11} \quad \text{(Ref. [12])}, \\ B_{\mu e}^{\mathrm{Ti}} &< 4.3 \times 10^{-12} \quad \text{(Ref. [13])}, \\ &< 4.6 \times 10^{-12} \quad \text{(Ref. [14])}, \\ B_{\mu e}^{\mathrm{Pb}} &< 4.9 \times 10^{-10} \quad \text{(Ref. [14])}. \end{aligned} \quad (2)$$

The signature of coherent $\mu \rightarrow e$ conversion is an electron emitted at the kinematical end point for bound muon decay, at 95.0 MeV for lead. Muonic atoms induce background not only through bound muon decay, but through radiative muon capture followed by asymmetric e^+e^- pair creation as well. Conversion events can be resolved from these intrinsic backgrounds for $B_{\mu e}$ values down to 10^{-14} if an instrumental resolution better than 2 MeV (FWHM) can be achieved [15]. Other potential sources of background originate from prompt beam-induced processes such as muon decay in flight, radiative pion capture, and electron scattering, and from cosmic rays.

The measurement was done at the μE1 beam line at PSI. Detailed information can be found in [16]. The SINDRUM II spectrometer consists of a set of concentric cylindrical detectors (Fig. 1 inside a superconducting solenoid. The muons enter the setup axially and traverse a CH_2 moderator and a plastic beam counter of 3.9 g/cm^2 overall thickness before reaching the target at the center. The lead target consists of 16 rectangular foils, 8 cm × 15 cm × 125 μm each, arranged radially with the 8 cm

 0031-9007/96/76(2)/200(4)$06.00

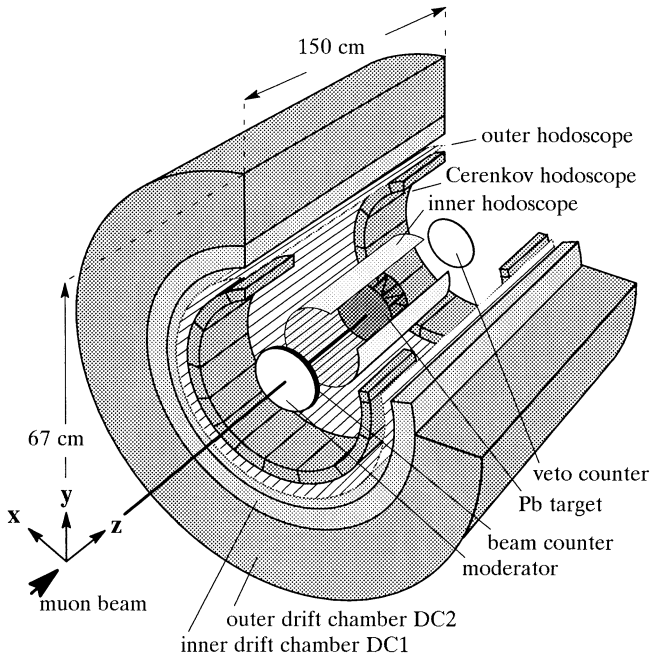

FIG. 1. Cutaway view of the SINDRUM II detection system. The spectrometer magnet is not shown.

sides welded to a 125 μm thick front cap and a 500 μm thick end cap; the total mass is 415 g.

The tracking region has a diameter of 1.3 m and a length of 1.5 m. Starting from the target decay particles traverse (i) at a radial distance of $r = 13.0$ cm an inner plastic scintillator hodoscope with 32 strips of 3 mm thickness and 80 cm length, (ii) at $r = 34.9$ cm an outer plastic scintillator hodoscope with 64 strips of 5 mm thickness and 150 cm length, (iii) between $r = 37.6$ and 44.5 cm the radial drift chamber DC1, (iv) between $r = 44.9$ and 64.8 cm the radial drift chamber DC2, and (v) at $r = 28.5$ cm, on both ends of the tracking region, two Čerenkov hodoscopes, each with 16 lucite elements of 30 mm thickness and 35 cm length. DC1 [17] is filled with CO_2/iC_4H_{10} (70/30), a slow drift gas with a Lorentz deflection angle of only 6° at 1.2 T. The sense wire plane is close to the outer wall, which is covered with cathode strips at 72° relative to the wires. The cathode signals give the position of the hits along the sense wires. The mean space resolution (σ) for typical events (see below) is 150 μm in the x-y plane and 1.3 mm in the z direction; see Fig. 1 for the definition of the coordinate system. DC2 is filled with He/iC_4H_{10} (88/12) with a radiation length of 1140 m. The x-y resolution is 1 mm.

At the field strength of 1.2 T charged particles leaving the target with transverse momenta below 100 MeV/c are contained radially inside the tracking region. The particles of interest cross the drift region of DC1 at least twice before reaching one of the two Čerenkov hodoscopes. The spectrometer response for $\mu \to e$ conversion was obtained by simulation [18]. The geometric acceptance was found to be (23.3 ± 0.4)%, which includes the losses by bremsstrahlung in the target.

To avoid background of scattered beam electrons, the muon channel was tuned to a momentum band of 90 ± 2 MeV/c, safely below the momentum of interest. The fraction of muons stopping in the target was (25 ± 5)%, as determined with the help of an additional beam counter positioned behind the target. Thanks to their shorter mean range the corresponding value for pions was only about 0.2%, which resulted in a pion contamination of order 10^{-7} in the target stops.

The trigger for data readout was based on the x-y hit pattern from the outer hodoscope and DC1 as expected for helical trajectories crossing the target and the DC1 sense wire plane. In addition, signals in the inner hodoscope and a Čerenkov hodoscope were required. The trigger efficiency for $\mu \to e$ events was found to be (50 ± 1)%, which includes detector efficiencies and deadtime in the trigger logic and the data-acquisition system.

During the measuring period of 10 days with an average beam rate of 1.0×10^7 μ^-/s, $N_{\text{stop}} = (2.1 \pm 0.4) \times 10^{12}$ muons stopped in the target, resulting in a raw data set of 8×10^5 events. The detector response was studied by stopping π^+ in a low-mass foam target and by measuring the trajectories of the 69.8 MeV positrons from the decay $\pi^+ \to e^+ \nu_e$. The magnetic field of the spectrometer was reversed and scaled in order to approximate the trajectories of conversion electrons as closely as possible.

In the off-line event analysis helical trajectories were searched and the momentum was fitted to the first two DC1 track elements. The reconstruction efficiency for events originating from the target region was (78 ± 3)%, mainly determined by the cathode efficiency of DC1. Field inhomogeneities, energy loss, and multiple scattering along the particle trajectory outside the target were taken into account. The resulting energy distribution of $\pi^+ \to e^+ \nu_e$ decays yields a resolution of 2.0% (FWHM), compared to 1.6% for the simulated events. The predicted resolution for conversion electrons is 2.8%. Since this value is dominated by the spread in energy loss in the lead target, the agreement between measurement and simulation should be much better in this case.

The reconstruction of the data sample with muon beam resulted in 7×10^4 electron events from the target region. 89% of them originate from electron scattering. This process is characterized by a narrow peak in the distribution of the time delay Δt between the spectrometer track and the preceding beam counter signal. The offset of Δt was chosen such that this peak is centered at $\Delta t = 0$ ns; muon decay in flight and radiative pion capture then peak at $\Delta t \approx 7$ ns. By requiring $\Delta t > 10$ ns more than 99% of the prompt electron and muon induced background and about 70% of the pion induced background was removed at the cost of a (22.6 ± 1.0)% loss of muonic-atom decays. Events induced by cosmic rays can be recognized by additional spectrometer signals. This background could be

reduced to a negligible level at the cost of a (9.8 ± 3.5)% loss of events of interest.

The resulting sample was interpreted within the framework of the extended likelihood method [19], which took into account (i) coherent $\mu \to e$ conversion (μe), (ii) muon decay in orbit ($\mu\nu$), (iii) scattering of beam electrons not recognized by the beam counter (ee'), and (iv) radiative pion capture ($\pi\gamma$) followed by e^+e^- pair creation in the target where the positron escaped detection. For $\mu\nu$ the theoretical energy distribution from Ref. [20] was assumed; the simulation of $\pi\gamma$ was based on the photon spectrum of Ref. [21].

The analysis was carried out in the five-dimensional distribution of total energy E_{tot}, delay Δt introduced above, z coordinate z_0 of the origin of the reconstructed trajectory relative to the front of the target, phase t_{rf} of the 50 MHz cyclotron-rf signal at decay time, and polar track angle θ. In the determination of the four density distributions the dependency on Δt, z_0, and t_{rf} was adjusted to the measured data.

In Fig. 2 the E_{tot} distribution of the selected events is compared with the distributions expected for the four processes. The hypothetical μe events can be distinguished from $\mu\nu$ events only by their different E_{tot} distribution. The energy distributions of $\mu\nu$ and ee' are quite similar; the latter process, however, is characterized by an asymmetric θ distribution and $8 < t_{\text{rf}} < 12$ ns. The $\pi\gamma$ events, finally, have a flat energy spectrum and steeply falling Δt and z_0 distributions caused by pions reaching the target with relatively low momenta.

The detector acceptance drops by an order of magnitude between 95 and 80 MeV, resulting in increased systematic uncertainties. For this reason the likelihood analysis was limited to the upper part of the energy distribution. A variation of the energy threshold between 80 and 86 MeV gave results for $B_{\mu e}$ which were stable to within ±2%. In the remainder of the text we quote the results for an energy threshold of 84 MeV. For this value the overall probability for a $\mu \to e$ conversion event to enter the final sample, given by the spectrometer acceptance and the various detector and selection efficiencies, was $\varepsilon_{\text{tot}} = (5.9 \pm 0.4)\%$.

The likelihood analysis gives for each event the probabilities P_i ($i = \mu e, \mu\nu, ee', \pi\gamma$) to be of event type i. Table I lists the characteristic observables and the resulting P_i values for the four main $\mu \to e$ candidates in the energy range between 88 and 95 MeV. According to the analysis it is most likely that three events are caused by radiative pion capture and one by electron scattering. No evidence for $\mu \to e$ conversion was found in this measurement.

Figures 3(a)–3(c) show two-dimensional projections of the extended likelihood function $\mathcal{L}(n_{\mu e}, n_{\mu\nu}, n_{ee'}, n_{\pi\gamma})$, where n_i denotes the number of events in channel i. In Fig. 3(d) the projection of $\mathcal{L}$ on $n_{\mu e}$ is shown, folded with the uncertainties in the assumed density distributions as described in Ref. [19]. From this function, and the three corresponding functions of $n_{\mu\nu}$, $n_{ee'}$, and $n_{\pi\gamma}$, one finds $0.7^{+2.2}_{-0.7}$ μe events, $13.6^{+4.0}_{-3.8}$ $\mu\nu$ events, $11.2^{+3.6}_{-2.5}$ ee' events, and $7.5^{+3.3}_{-1.9}$ $\pi\gamma$ events, which may be compared with 12 ± 4 $\mu\nu$ events predicted by the simulation, 12 ± 3 ee' events found in the t_{rf} peak, and 6 $\pi\gamma$ events observed in the corresponding positron distribution. The upper limit on $n_{\mu e}$ is $n_{\mu e}^{\max} = 5.1$ (90% C.L.). The upper limit on the branching ratio is calculated following Ref. [22]:

$$B_{\mu e} < \frac{n_{\mu e}^{\max}[1 + (n_{\mu e}^{\max} - \hat{n}_{\mu e})\sigma_r^2/2]}{f_{\text{capt}} N_{\text{stop}} \varepsilon_{\text{tot}}}, \qquad (3)$$

where the capture probability f_{capt} has been discussed in the introduction, $\hat{n}_{\mu e} = 0.7$ is the value of $n_{\mu e}$ where $\mathcal{L}$ reaches its maximum, and $\sigma_r = 0.21$ is the relative uncertainty in $N_{\text{stop}}\varepsilon_{\text{tot}}$. The result for the branching ratio of $\mu \to e$ conversion on lead is

$$B_{\mu e}^{\text{Pb}} < 4.6 \times 10^{-11} \text{ (90\% C.L.)}, \qquad (4)$$

which improves on the previous upper limit [14] by an order of magnitude. Combined with the 4.3×10^{-12} limit for titanium [13] this yields the following 90% C.L. on the

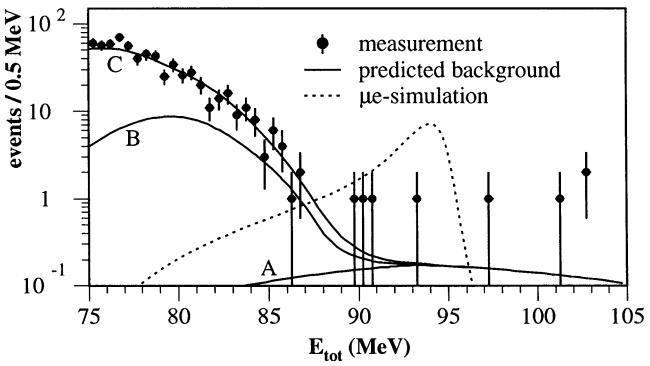

FIG. 2. Energy spectra for electrons from the target. Prompt beam-correlated events and cosmic ray background have been rejected. The measured distribution is compared with predicted distributions for $\pi\gamma$ (*A*), $\pi\gamma + ee'$ (*B*), and $\pi\gamma + ee' + \mu\nu$ (*C*), discussed in the text. For the simulation of $\mu \to e$ conversion $B_{\mu e} = 4.9 \times 10^{-10}$ was assumed, which corresponds to the limit of Ref. [14].

TABLE I. Values of the five kinematic observables used in the likelihood analysis and probabilities to belong to one of the four event types considered in the analysis, for the four main $\mu \to e$ candidates.

E_{tot} (MeV)	Δt (ns)	z_0 (cm)	t_{rf} (ns)	θ (deg)	P_i (%) μe	$\mu\nu$	ee'	$\pi\gamma$
89.9	10.7	9.1	4.0	65	7	26	0	67
90.2	21.1	3.2	13.2	72	7	14	0	79
90.9	155.8	16.3	11.8	70	32	20	48	0
93.0	26.9	0.9	1.5	102	19	0	0	81

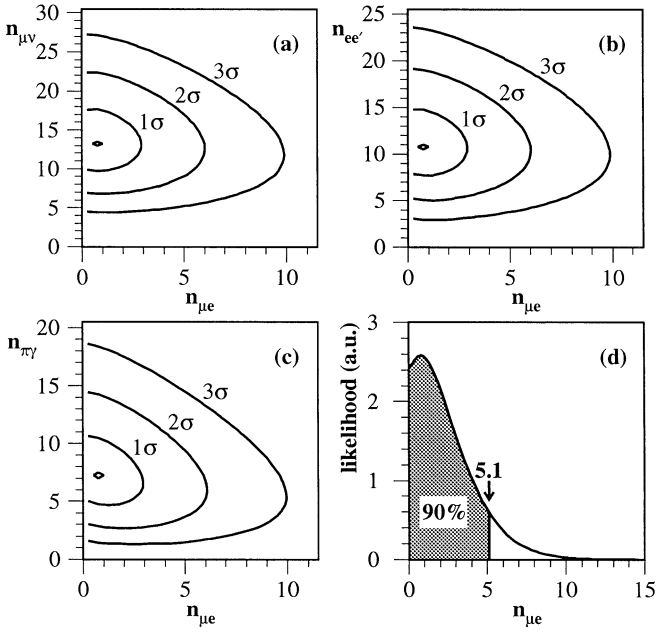

FIG. 3. Extended likelihood function $\mathcal{L}(n_{\mu e}, n_{\mu\nu}, n_{ee'}, n_{\pi\gamma})$ for the data sample with $E_{\text{tot}} > 84$ MeV. (a)–(c) Two-dimensional projections of $\mathcal{L}$ on $n_{\mu e}$ and each of $n_{\mu\nu}$, $n_{ee'}$, and $n_{\pi\gamma}$. (d) The projection of $\mathcal{L}$ on $n_{\mu e}$. The latter distribution has its maximum at $n_{\mu e} = 0.7$, whereas the 90% confidence upper limit is reached at $n_{\mu e}^{\max} = 5.1$.

coupling constants introduced in Eq. (1):

$$\begin{aligned} |g_V^0| &< 3.9 \times 10^{-7}, \qquad |g_V^1| < 9.7 \times 10^{-6}, \\ |g_S^0| &< 5.2 \times 10^{-7}, \qquad |g_S^1| < 1.4 \times 10^{-5}. \end{aligned} \tag{5}$$

As is shown in Fig. 4 for g_V^0 and g_V^1, the allowed regions are correlated.

The SINDRUM II experiment aims at a final sensitivity to $B_{\mu e}$ of a few times 10^{-14}. For this purpose a dedicated muon channel is presently under construction at PSI. The measurement on titanium mentioned above [13] was meanwhile continued at the existing beam line. Analysis of these data is in progress.

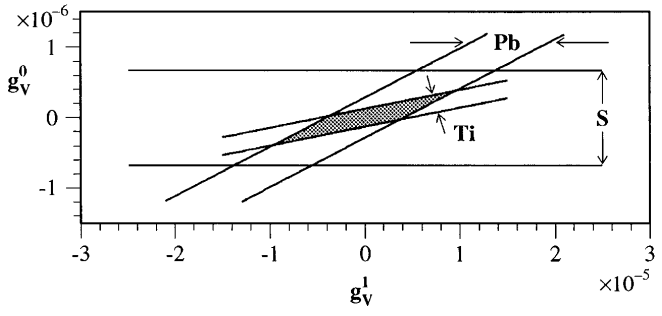

FIG. 4. Allowed region for g_V^0 and g_V^1, the isoscalar and isovector coupling constants for vector interaction, as defined by Eq. (1). The constraints come from the experimental upper limits on $B_{\mu e}$ for sulfur 12, titanium 13, and lead (this work).

This work was supported in part by the Bundesministerium für Bildung, Wissenschaft, Forschung und Technologie, Germany, under Contract No. 06AC651 and by the Swiss National Science Foundation.

*Present address: PSI, CH-5232 Villigen PSI, Switzerland.
†Present address: DESY, IfH Zeuthen, D-15738 Zeuthen, Germany.
‡Permanent address: Institute for Nuclear Studies, PL-05-400 Swierk, Poland.
§Present address: DESY, D-22607 Hamburg, Germany.

[1] J. D. Vergados, Phys. Rep. **133**, 1 (1986).
[2] A. van der Schaaf, in *Progress in Particle and Nuclear Physics*, edited by A. Faessler (Pergamon, Oxford, 1993), Vol. 31, p. 1.
[3] P. Depommier and C. Leroy, Rep. Prog. Phys. **58**, 61 (1995).
[4] G. Altarelli *et al.*, Nucl. Phys. **B125**, 285 (1977).
[5] O. Shanker, Nucl. Phys. **B206**, 253 (1982).
[6] R. N. Cahn and H. Harari, Nucl. Phys. **B176**, 135 (1980).
[7] J. Bernabéu *et al.*, Nucl. Phys. **B409**, 69 (1993).
[8] L. N. Chang *et al.*, Phys. Rev. D **50**, 4589 (1994).
[9] T. Suzuki and D. F. Measday, Phys. Rev. C **35**, 2212 (1987).
[10] H. C. Chiang *et al.*, Nucl. Phys. **A559**, 526 (1993).
[11] O. Shanker, Phys. Rev. D **20**, 1608 (1979).
[12] A. Badertscher *et al.*, Nucl. Phys. **A377**, 406 (1982).
[13] SINDRUM II Collaboration, C. Dohmen *et al.*, Phys. Lett. B **317**, 631 (1993).
[14] S. Ahmad *et al.*, Phys. Rev. D **38**, 2102 (1988).
[15] A. van der Schaaf (spokesman), PSI proposal R-87-03, 1987.
[16] W. Honecker, Ph.D. thesis, RWTH, Aachen, Germany [Inst. Report No. PITHA/66, 1994 (unpublished)].
[17] M. Grossmann-Handschin *et al.*, Nucl. Instrum. Methods Phys. Res., Sect. A **327**, 378 (1993).
[18] GEANT, CERN Program Library Long Write-up W5013, Geneva, Switzerland, 1993.
[19] V. Innocente and L. Lista, Nucl. Instrum. Methods Phys. Res., Sect. A **340**, 396 (1994).
[20] R. Watanabe *et al.*, At. Data Nucl. Data Tables **54**, 165 (1993).
[21] H. W. Baer, in *Proceedings of the 7th International Conference on High-Energy Physics and Nuclear Structure*, edited by M. P. Locher (Birkhäuser, Basel/Stuttgart, 1977), p. 245.
[22] R. D. Cousins and V. L. Highland, Nucl. Instrum. Methods Phys. Res., Sect. A **320**, 331 (1992).